


Time-Frequency Spectroscopy of GaAs Transient Dispersion Using Few-Cycle Pump-Probe Reflectometry

Hemang Jani  and Lingze Duan *

Department of Physics & Astronomy, The University of Alabama in Huntsville, Huntsville, Alabama 35899, USA

 (Received 24 September 2019; revised manuscript received 23 February 2020; accepted 13 April 2020; published 5 May 2020)

The rapid development of new photonic materials calls for simple yet effective approaches to characterize ultrafast dynamics in materials and devices. Here we demonstrate time-frequency transient reflectometry based on a compact, few-cycle pump-probe reflectometer. The system simultaneously features a broad spectral range (300 nm) and fine temporal resolution (10 fs), and it requires only a femtosecond oscillator. With this capability, we report a time-frequency spectroscopic measurement of the transient dispersion of GaAs near its band gap. Our results map important carrier dynamics such as carrier cooling, carrier decay, band filling, and band-gap renormalization on a single two-dimensional graph, offering a comprehensive picture of these processes and revealing details unattainable with conventional methods.

DOI: [10.1103/PhysRevApplied.13.054010](https://doi.org/10.1103/PhysRevApplied.13.054010)

I. INTRODUCTION

Over the last decade, advances in novel materials such as two-dimensional (2D) materials, metamaterials, plasmonic materials, and negative-electron-affinity structures, have triggered rapid growth in the development of ultrafast optoelectronic devices [1–4]. This sparks an urgent demand for techniques capable of characterizing ultrafast carrier dynamics in such devices [5–8]. Transient processes such as carrier relaxation and carrier transportation near device surfaces are especially important to the operation of many ultrafast devices, including negative-electron-affinity photocathodes [7], fast photoconductive switches [8], and photodetectors based on 2D materials [9]. Comprehensive study of these processes requires time-resolved, broadband reflective spectroscopy with femtosecond-scale temporal resolution.

Optical reflectometry is a versatile diagnostic technique that is often used to characterize optical constants such as the index of refraction and the group index [10,11]. Combining the concept of optical reflectometry with the femtosecond pump-probe method leads to pump-probe reflectometry (PPR), a technique especially capable of characterizing ultrafast optical properties [12]. In a typical PPR scheme, the surface reflectivity of a device sample is measured at various time delays after the material is optically excited by energetic “pump” pulses [12–16]. Since the transient variation of reflectivity is determined by the transient variation of the dielectric constant, which in turn is strongly influenced by the evolution of the free-carrier

population after optical excitation, PPR is able to provide a direct picture of ultrafast carrier dynamics inside the material [13,14,16]. Compared with other time-resolved techniques such as ultrafast luminescence spectroscopy [17] and time-resolved photoelectron spectroscopy [18], PPR is easier to realize experimentally and better suited for studying semiconductor devices [19].

Most of the PPR experiments reported so far were designed either for narrow-band, time-domain measurement [13–16] or broadband, spectral-domain measurement [20–22]. In the case of time-domain PPR, the time evolution of the total reflected power is measured. This approach is schematically simple and often requires only a femtosecond oscillator as the light source [13]. The standard pulse width in time-domain PPR ranges between 30 and 100 fs and the typical spectral width is 20–60 nm [15,16]. Because of the relatively narrow spectral range, the measured transient reflectivity represents only a portion of the overall dielectric function near the center wavelength. Such a drawback can be partially addressed by use of a wavelength-tunable mode-locked laser, which provides an extra dimension to expand the spectral coverage [13]. However, from a practical point of view, tuning the laser wavelength is often unreliable and difficult, and in some cases even not feasible.

Meanwhile, broadband, spectral-domain PPR can be achieved by broadening the probe pulses into “white light” and measuring the spectral response of transient reflectivity via a spectrometer. This allows the full dielectric function to be characterized within a broad wavelength range (hundreds of nanometers) [12], which provides far-more insight into the carrier dynamics than a simple

*lingze.duan@uah.edu

time-domain measurement. The advent of nonlinear photonic crystal fiber in recent years has also significantly lowered the power requirement for generating such super-continuum probes [23,24]. This method, however, has a key weakness: its temporal resolution is often compromised during the nonlinear-spectral-broadening process [21,22,24]. Although temporal-resolution recovery with strongly chirped pulses is possible under certain circumstances [25], the required conditions (e.g., narrowband sample absorption) are not always satisfied with photonic materials, and it is unclear if the technique can be applied under strong nonlinear spectral broadening. Moreover, in many cases, multistage optical amplifiers are also needed to perform spectral-domain measurement [12,21], considerably increasing the cost, size, and complexity of the system.

In the work reported here, we seek to develop a PPR system with both high temporal resolution and broad spectral coverage. Such capabilities were demonstrated previously with the use of chirped-pulse amplification and nonlinear optical parametric amplifiers [26], which led to a high baseline cost and high system complexity (albeit with the additional feature of a tunable pump). Our approach is based on a simple design featuring a few-cycle femtosecond laser and an ultrabroadband pump-probe system. The unique design of the pump-probe system allows the pulse width and the spectrum of the laser to be preserved throughout the beam paths and eventually delivered onto

the sample. The result is a low-cost (oscillator-only), compact (small-footprint) pump-probe reflectometer that can make time-domain and spectral-domain measurements simultaneously. In the second part of the paper, the capability of this reflectometer is demonstrated by time-frequency spectroscopy of the transient dispersion (TD) of GaAs near its band gap. Our results show that, even for a material as well studied as GaAs, few-cycle PPR can offer new insights into the ultrafast carrier dynamics.

II. FEW-CYCLE PUMP-PROBE REFLECTOMETER

Our PPR system is built around a 6-fs Ti:sapphire oscillator (Venteon Pulse:One), which offers an average power of 500 mW at a repetition rate of 83 MHz. The laser is integrated in a portable pump-probe platform as depicted in Fig. 1. Special measures are taken to manage pulse dispersion throughout the beam paths so that the optimum pulse shape can be achieved on the sample surface. These include the use of a pair of dispersion-compensating mirrors at the output of the laser to precompensate the group-velocity dispersion introduced by air and glass during pulse transmission. A CaF₂ wedge pair inserted after the DCMs provides fine dispersion tuning. An 1-mm-thick ultrabroadband, dispersion-balanced beam splitter splits the laser output into pump and probe beams. Its special coating produces low group-delay dispersion in

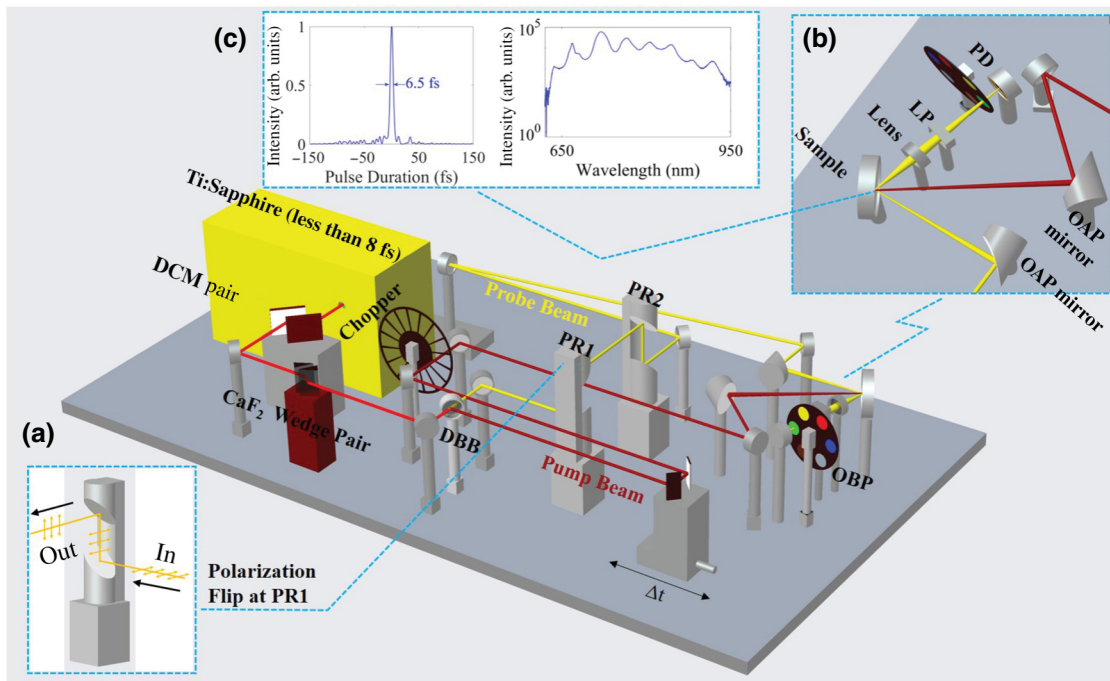


FIG. 1. Layout of the PPR setup: (a) polarization rotation by a periscope; (b) enlarged view of the detection system. (c) Time-domain and frequency-domain characterization of the pump pulse. DBB, dispersion-balance beam splitter; DCM, dispersion-compensating mirror; LP, linear polarizer; OAP, off-axis parabolic; OBP, optical bandpass filter; PD, photodetector; PR, periscope.

both transmission and reflection with similar spectral profiles, which allow simultaneous dispersion compensation for both pump pulses and probe pulses. Except for the DCMs, the CaF₂ wedge, and the dispersion-balanced beam splitter, all the optics used in the beam path before the sample are reflective components with protected silver coatings. The pump beam, which has an average power of 270 mW, passes through a motorized tunable delay line (Newport VP-25XA) and a beam chopper before being focused onto the sample at near-normal incidence by an off-axis parabolic mirror. The probe beam has an average power of 20 mW. Its polarization is rotated by 90° through a periscope, as seen in Fig. 1(a). A second off-axis parabolic mirror then focuses the beam onto the sample at 15°. The probe spot size on the sample surface is about one third of the pump spot size. The probe beam reflected off the sample surface is focused onto a Si photodetector, and the detector output feeds into a lock-in amplifier (SRS SR830). Wavelength selectivity is introduced to the probe measurement through the addition of a tunable optical bandpass filter in front of the photodetector. A polarizer is inserted before the bandpass filter to remove residual pump light in the reflected probe signal. An enlarged view of the detection section is shown in Fig. 1(b). The overall footprint of the setup (excluding the laser) is $72 \times 45 \text{ cm}^2$.

The pump pulses are characterized at the location of the sample by spectral-phase interferometry for direct electric-field reconstruction (SPIDER). The time-domain and frequency-domain results are shown in Fig. 1(c). A pulse duration of 6.5 fs full width at half maximum and a spectral width of 300 nm at 20 dB below the peak are obtained. A portion of the probe beam is split off by the beam splitter and is coupled into a spectrometer (Ocean Optics USB2000) for real-time measurement of the probe spectrum. This spectral information is used to normalize the measured reflectivity spectra to take into account the different incident powers at different wavelengths. The probe-pulse width is estimated to be about 10 fs.

III. TRANSIENT DISPERSION OF GaAs

To demonstrate the capability of few-cycle PPR, we perform time-frequency measurement of the transient dispersion of GaAs. Ultrafast carrier dynamics in GaAs has long been a focus of research due to its potential impact on the performances of photonic devices. One important aspect of such dynamics is carrier-induced TD, which characterizes the ultrafast change of the refractive index near the band gap due to the injection and relaxation of photocarriers [27–29]. Fundamentally, TD serves as a manifestation of several important many-body effects in semiconductors, including band filling, band-gap renormalization, free-carrier absorption, and plasma screening [16,30–32]. Practically, TD has proved to be a key mechanism underlying some of the dynamic properties of

optoelectronic devices [33–35]. A complete characterization of TD requires time-frequency measurement of the transient reflectivity. However, despite continued effort in both the time domain [36–39] and the frequency domain [12,22], there has been no report of direct observation of time-frequency behaviors of TD near the GaAs band gap.

Few-cycle PPR offers a comprehensive approach to study the TD of GaAs. Using the reflectometer shown in Fig. 1, we measure the transient reflectivity of GaAs at a series of probe wavelengths over a range of 200 nm across the band gap. The sample used in this measurement is a 0.35-mm Si-doped GaAs wafer (110) with a doping concentration of $3 \times 10^{18} \text{ cm}^{-3}$. Figure 2(a) shows several representative PPR traces at various wavelengths. The wavelength selection is accomplished via the change of the center wavelength of the tunable bandpass filter in front of the detector. The PPR traces show diverse behaviors of the refractive index at different wavelengths, highlighted by their different peak values as well as the corresponding rise times. Such differences become even more obvious

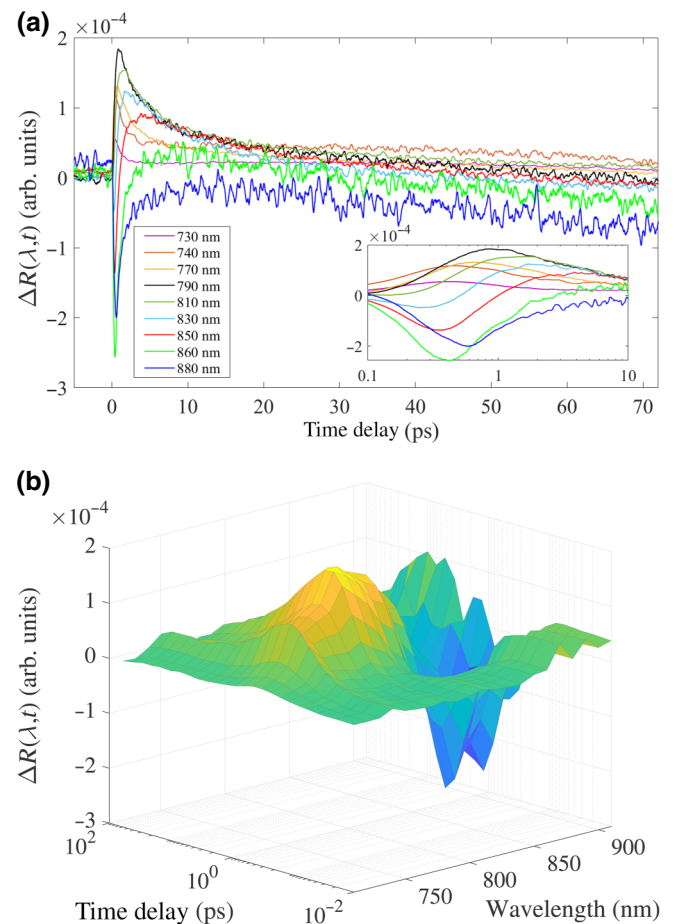


FIG. 2. (a) PPR traces at various probe wavelengths show a range of peak reflectivities and rise times. (b) A time-frequency spectrogram of GaAs covers a 200-nm spectral range and almost four decades of the timescale (10 fs – 50 ps).

when the traces are plotted on a semilog scale, as shown in the inset in Fig. 2. The transient reflectivity switches sign across the band gap. This is due to refractive-index nonlinearity near the GaAs band gap [28], and is consistent with prior observations [36,37]. A bipolar behavior of the index is observed near the band gap (810–860 nm), which is also consistent with theoretical predictions [29].

By assembling all these individual PPR traces of different wavelengths together, we obtain a full time-frequency map of the transient reflectivity $\Delta R(\lambda, t)$, as shown in Fig. 2(b). A 10-nm wavelength increment is used in the measurement. This wavelength resolution is limited by the available bandpass filters but should be easily increased with continuously tunable optical bandpass filters [40]. Since $\Delta R(\lambda, t)$ is proportional to the refractive index $\Delta n(\lambda, t)$ [37], Fig. 2(b) effectively presents a time-frequency spectrogram of TD. Compared with conventional PPR [12,36–39], time-frequency measurement offers a comprehensive picture of the ultrafast evolution of the dielectric constant due to carrier injection and relaxation.

The time-frequency spectrogram shown in Fig. 2(b) can be better analyzed by projecting the distribution of $\Delta R(\lambda, t)$ onto a 2D contour plot as shown in Fig. 3(a). The resulting topographic map features a prominent “arch” region that spans diagonally across the middle, indicating a rise of reflectivity (and hence refractive index) above the steady-state value. It begins to emerge at about 200 fs and extends to above 10 ps. The diagonal pattern suggests that the refractive index for longer wavelengths peaks at later times. Meanwhile, a “sag” region can be seen at the lower right, signifying a dip of the index function below its steady-state values. This region has a similar diagonal pattern but begins to appear at a much earlier time (50 fs). The existence of these two regions indicates a

bipolar nature of the carrier-induced index change $\Delta n(\lambda)$ as a function of wavelength. This becomes more evident when we plot $\Delta n(\lambda)$ at several different time delays as shown in Fig. 3(b). Such a characteristic agrees well with theoretical models based on the combined effects of band filling and band-gap renormalization [28,29]. In particular, the early appearance of the sag region below the band gap appears to be consistent with theory and prior experiments, which shows that the negative change of the index below the band gap is more prominent than the positive change above the band gap [28]. Although the above results are obtained with one particular sample, similar characteristics are observed on several other GaAs samples with different orientations and doping levels.

The TD spectrogram also reveals some interesting details about the behaviors of the transition edge. The transition edge is seen in Fig. 3(a) as the narrow strip between the arch region and the sag region. It is where the index change crosses zero [see Fig. 3(b)] and is an important indicator of the carrier dynamics. To highlight the time evolution of the transition edge, a rough guideline is included in Fig. 3(a). Immediately following the injection of the pump pulse, no visible change of the refractive index is detected. It is only after about 50 fs that the index change begins to appear. From 50 to 200 fs, this change is primarily in the form of a depression below the band gap. From the boundary of this sag region, it is reasonable to conceive that the transition edge experiences a blueshift within this time range. At about 200 fs, the index function above the band gap begins to grow, while its counterpart below the band gap continues to decrease. A clear transition edge is formed. What is interesting about this transition edge is that it turns to the opposite direction and begins to veer toward longer wavelengths. The redshift lasts for about

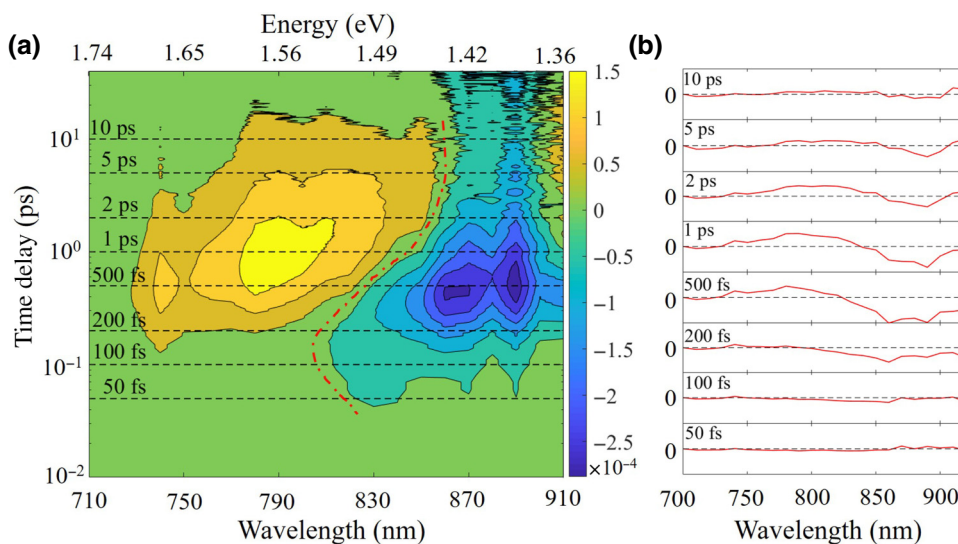


FIG. 3. (a) Time-frequency map of the transient dispersion $\Delta n(\lambda, t)$ of GaAs under few-cycle excitation. The dash-dotted curve outlines the evolution of the transition edge. (b) Cutout views of the index function at different delay times.

5 ps and covers the wavelength range from 810 to 860 nm. Then the transition edge stabilizes at 860 nm, which is very close to the steady-state band gap of the sample.

IV. DISCUSSION

While a thorough theoretical analysis is beyond the scope of this paper, it is instructive to put the above observation into the context of carrier relaxation and decay. According to semiconductor theories [19,41,42], ultrafast carrier dynamics following the excitation by a femtosecond laser pulse includes three key processes. The first one is momentum randomization, where carrier-carrier scattering allows the photoexcited carriers to thermalize into a Fermi-Dirac distribution. This process typically occurs within the first tens of femtoseconds. The second one is energy relaxation (or carrier cooling). This is when carrier-phonon scattering causes energy exchange between the “hot” carriers and the lattice. The carriers eventually reach thermal equilibrium with the lattice and relax to the bottom (top) of the conduction (valence) band. This process typically occurs on a timescale of several picoseconds. The third one is carrier decay. During this process, various decay mechanisms (e.g., recombination, capture, diffusion) cause the population of photoexcited carriers to reduce. Depending on which mechanism dominates, the timescale of this process can range from less than 1 ps to nanoseconds.

Putting the above behaviors of TD into this theoretical framework leads to a phenomenological picture of the underlying physics, which can be viewed from two aspects: (i) the magnitude of the index modulation and (ii) the spectral shift of the transition edge. The peak value of the index modulation is an indication of free-carrier density [28]. Within the first few femtoseconds following the pump pulse, the hot photocarriers are in a highly nonequilibrium state with large kinetic energies [43,44]. It is only after they fully thermalize and start to reach equilibrium with the surroundings that they begin to contribute to the dielectric properties of the material. This is why in Fig. 3 measurable index modulation appears about 50 fs after the pump excitation. As more and more carriers cool down and fill the lower-energy states, the index modulation continues to grow (from 50 fs to 1 ps), signifying a growing population of equilibrated photocarriers. The free-carrier density peaks at about 1 ps. Then carrier decay and, possibly, carrier diffusion [45] take over and gradually lower the free-carrier population, as is evident from the reducing modulation of the index function after 1 ps [see Fig. 3(b)]. The carrier-induced index modulation eventually tapers off after about 10 ps.

Meanwhile, the spectral shift of the transition edge indicates changes occurred to the band gap. It is worth noting here that the transient behavior of the band gap is under the influence of two competing processes: band filling, which

causes the band gap to grow (blue shift) and band-gap renormalization, which leads to band-gap shrinkage (red shift). With this understanding, the initial blueshift of the transition edge between 50 and 200 fs appears to indicate that, between the two processes, band filling has an effect first and dominates in the early stage of carrier cooling. Then band-gap renormalization gradually sets in and eventually becomes the prevailing effect. This is evident from the reversal of the band-gap shift after 200 fs. The delayed appearance of band-gap renormalization relative to band filling suggests that band-gap renormalization requires a higher degree of carrier equilibrium to commence, which takes a longer time to develop. This is conceivable because band-gap renormalization relies on the collective effect of Coulomb screening of many particles to be established [29]. Such a state requires a buildup time typically on the order of 50–200 fs according to both theoretical predictions [46,47] and experimental observations [48]. From this point of view, the reversal of the band-gap shift offers direct evidence of different onset times between band filling and band-gap renormalization when the carrier state transitions from a nonequilibrium state to an equilibrium state.

V. CONCLUSION

In conclusion, we develop of a compact, few-cycle pump-probe reflectometer. As a proof-of-concept demonstration, we perform time-frequency spectroscopy of the transient dispersion of GaAs near its band gap. The time-frequency spectrogram maps key carrier dynamics onto a single 2D graph, showing a movielike chronicle of transient carrier behaviors in GaAs with 10-fs resolution. It reveals a reversal of the band-gap shift within the first few hundred femtoseconds after pump excitation, showing evidence of different characteristics of band filling and band-gap renormalization during the process of carrier equilibration. This highlights the capability of few-cycle PPR; that is, even for a material as well studied as GaAs, the technique can offer new insights into its ultrafast dynamics.

ACKNOWLEDGMENTS

We acknowledge the support of Mr. Ted Rogers of the Center for Applied Optics for his help with the diagram of the optical system. This work received funding from the National Science Foundation (Grants No. ECCS-1254902 and No. ECCS-1606836).

-
- [1] F. Xia, H. Wang, D. Xiao, M. Dubey, and A. Ramasubramaniam, Two-dimensional material nanophotonics, *Nat. Photonics* **8**, 899 (2014).

- [2] A. Krasnok, M. Tymchenko, and A. Alu, Nonlinear metasurfaces: A paradigm shift in nonlinear optics, *Mater. Today* **21**, 8 (2018).
- [3] A. Pors, M. G. Nielsen, and S. I. Bozhevolnyi, Broadband plasmonic half-wave plates in reflection, *Opt. Lett.* **38**, 513 (2013).
- [4] J. Zou, X. Ge, Y. Zhang, W. Deng, Z. Zhu, W. Wang, X. Peng, Z. Chen, and B. Chang, Negative electron affinity GaAs wire-array photocathodes, *Opt. Express* **24**, 4632 (2016).
- [5] M. Mrejen, U. Arieli, A. Levanon, and H. Suchowski, in *CLEO: QELS Fundamental Science* (Optical Society of America, San Jose, CA, 2017), p. FW4H-2.
- [6] P. Steinleitner, P. Merkl, P. Nagler, J. Mornhinweg, C. Schuller, T. Korn, A. Chernikov, and R. Huber, Direct observation of ultrafast exciton formation in a monolayer of WSe₂, *Nano Lett.* **17**, 1455 (2017).
- [7] A. Feng, L. Yin, S. Zhang, L. Chen, Y. Qian, H. Jani, and L. Duan, Femtosecond pump-probe spectroscopy investigation of carrier dynamics in GaAlAs photocathodes, *Optik* **179**, 336 (2019).
- [8] L. Deng, W. Zhu Lin, Z. Rong Sun, and Z. Geng Wang, Response characteristic of femtosecond LT-GaAs photoconductive switches at different voltage biases, *J. Phys. D: Appl. Phys.* **42**, 245103 (2009).
- [9] F. Koppens, T. Mueller, P. Avouris, A. Ferrari, M. Vitiello, and M. Polini, Photodetectors based on graphene, other two-dimensional materials and hybrid systems, *Nat. Nanotechnol.* **9**, 780 (2014).
- [10] G. Kerr, R. Hamm, M. Williams, R. Birkhoff, and L. Painter, Optical and dielectric properties of water in the vacuum ultraviolet, *Phys. Rev. A* **5**, 2523 (1972).
- [11] W. Sorin and D. Gray, Simultaneous thickness and group index measurement using optical low-coherence reflectometry, *IEEE Photonics Technol. Lett.* **4**, 105 (1992).
- [12] C. Roeser, A.-T. Kim, J. Callan, L. Huang, E. Glezer, Y. Siegal, and E. Mazur, Femtosecond time-resolved dielectric function measurements by dual-angle reflectometry, *Rev. Sci. Instrum.* **74**, 3413 (2003).
- [13] T. Tanaka, A. Harata, and T. Sawada, Subpicosecond surface-restricted carrier and thermal dynamics by transient reflectivity measurements, *J. Appl. Phys.* **82**, 4033 (1997).
- [14] A. Sabbah and D. M. Riffe, Femtosecond pump-probe reflectivity study of silicon carrier dynamics, *Phys. Rev. B* **66**, 165217 (2002).
- [15] T. Korn, A. Franke-Wiekhorst, S. Schnüll, and I. Wilke, Characterization of nanometer as-clusters in low-temperature grown GaAs by transient reflectivity measurements, *J. Appl. Phys.* **91**, 2333 (2002).
- [16] N. P. Wells, P. M. Belden, J. R. Demers, and W. T. Lotshaw, Transient reflectivity as a probe of ultrafast carrier dynamics in semiconductors: A revised model for low-temperature grown GaAs, *J. Appl. Phys.* **116**, 073506 (2014).
- [17] T. Elsaesser, J. Shah, L. Rota, and P. Lugli, Initial Thermalization of Photoexcited Carriers in GaAs Studied by Femtosecond Luminescence Spectroscopy, *Phys. Rev. Lett.* **66**, 1757 (1991).
- [18] A. Stolow, A. E. Bragg, and D. M. Neumark, Femtosecond time-resolved photoelectron spectroscopy, *Chem. Rev.* **104**, 1719 (2004).
- [19] A. Othonos, Probing ultrafast carrier and phonon dynamics in semiconductors, *J. Appl. Phys.* **83**, 1789 (1998).
- [20] C. Shank, R. Yen, and C. Hirlimann, Time-Resolved Reflectivity Measurements of Femtosecond-Optical-Pulse-Induced Phase Transitions in Silicon, *Phys. Rev. Lett.* **50**, 454 (1983).
- [21] M. Downer and C. Shank, Ultrafast Heating of Silicon on Sapphire by Femtosecond Optical Pulses, *Phys. Rev. Lett.* **56**, 761 (1986).
- [22] L. Huang, J. P. Callan, E. N. Glezer, and E. Mazur, GaAs Under Intense Ultrafast Excitation: Response of the Dielectric Function, *Phys. Rev. Lett.* **80**, 185 (1998).
- [23] J. M. Dudley and J. R. Taylor, Ten years of nonlinear optics in photonic crystal fibre, *Nat. Photonics* **3**, 85 (2009).
- [24] J. Léonard, N. Lecong, J.-P. Likforman, O. Crégut, S. Haacke, P. Viale, P. Leproux, and V. Couderc, Broadband ultrafast spectroscopy using a photonic crystal fiber: Application to the photophysics of malachite green, *Opt. Express* **15**, 16124 (2007).
- [25] D. Polli, D. Brida, S. Mukamel, G. Lanzani, and G. Cerullo, Effective temporal resolution in pump-probe spectroscopy with strongly chirped pulses, *Phys. Rev. A* **82**, 053809 (2010).
- [26] D. Polli, L. Lüer, and G. Cerullo, High-time-resolution pump-probe system with broadband detection for the study of time-domain vibrational dynamics, *Rev. Sci. Instrum.* **78**, 103108 (2007).
- [27] F. Stern, Dispersion of the index of refraction near the absorption edge of semiconductors, *Phys. Rev.* **133**, A1653 (1964).
- [28] Y.-H. Lee, A. Chavez-Pirson, S. W. Koch, H. Gibbs, S. Park, J. Morhange, A. Jeffery, N. Peyghambarian, L. Banyai, A. Gossard, and W. Wiegmann, Room-Temperature Optical Nonlinearities in GaAs, *Phys. Rev. Lett.* **57**, 2446 (1986).
- [29] B. R. Bennett, R. A. Soref, and J. A. Del Alamo, Carrier-induced change in refractive index of InP, GaAs and InGaAsP, *IEEE J. Quantum Electron.* **26**, 113 (1990).
- [30] R. Abram, G. Childs, and P. Saunderson, Band gap narrowing due to many-body effects in silicon and gallium arsenide, *J. Phys. C: Solid State Phys.* **17**, 6105 (1984).
- [31] S. Prabhu and A. Vengurlekar, Dynamics of the pump-probe reflectivity spectra in GaAs and GaN, *J. Appl. Phys.* **95**, 7803 (2004).
- [32] V. Ortiz, J. Nagle, J.-F. Lampin, E. Peronne, and A. Alexandrou, Low-temperature-grown GaAs: Modeling of transient reflectivity experiments, *J. Appl. Phys.* **102**, 043515 (2007).
- [33] S. Tarucha, H. Kobayashi, Y. Horikoshi, and H. Okamoto, Carrier-induced energy-gap shrinkage in current-injection GaAs/AlGaAs mqw heterostructures, *Jpn. J. Appl. Phys.* **23**, 874 (1984).
- [34] C. Ell, H. Haug, and S. W. Koch, Many-body effects in gain and refractive-index spectra of bulk and quantum-well semiconductor lasers, *Opt. Lett.* **14**, 356 (1989).
- [35] C.-F. Hsu, P. S. Zory, C.-H. Wu, and M. A. Emanuel, Coulomb enhancement in InGaAs-GaAs quantum-well lasers, *IEEE J. Sel. Top. Quantum Electron.* **3**, 158 (1997).

- [36] T. Gong, W. Nighan, Jr., and P. Fauchet, Hot-carrier coulomb effects in GaAs investigated by femtosecond spectroscopy around the band edge, *Appl. Phys. Lett.* **57**, 2713 (1990).
- [37] F. Ganikhanov, G.-R. Lin, W.-C. Chen, C.-S. Chang, and C.-L. Pan, Subpicosecond carrier lifetimes in arsenic-ion-implanted GaAs, *Appl. Phys. Lett.* **67**, 3465 (1995).
- [38] S. Janz, U. G. Akano, and I. V. Mitchell, Nonlinear optical response of As⁺-ion implanted GaAs studied using time resolved reflectivity, *Appl. Phys. Lett.* **68**, 3287 (1996).
- [39] R. Yano, Y. Hirayama, S. Miyashita, H. Sasabu, N. Uesugi, and S. Uehara, Pump-probe spectroscopy of low-temperature grown GaAs for carrier lifetime estimation: Arsenic pressure dependence of carrier lifetime during MBE crystal growth, *Phys. Lett. A* **289**, 93 (2001).
- [40] M.-Y. Jeong and J. Y. Mang, Continuously tunable optical notch filter and band-pass filter systems that cover the visible to near-infrared spectral ranges, *Appl. Opt.* **57**, 1962 (2018).
- [41] A. M.-T. Kim, Ph.D. thesis, Citeseer (2001).
- [42] R. R. Alfano, *Semiconductors Probed by Ultrafast Laser Spectroscopy* (Academic Press, New York, 1984).
- [43] R. Schoenlein, W. Lin, E. Ippen, and J. Fujimoto, Femtosecond hot-carrier energy relaxation in GaAs, *Appl. Phys. Lett.* **51**, 1442 (1987).
- [44] H. Tanimura, J. Kanasaki, K. Tanimura, J. Sjakste, N. Vast, M. Calandra, and F. Mauri, Formation of hot-electron ensembles quasiequilibrated in momentum space by ultrafast momentum scattering of highly excited hot electrons photoinjected into the Γ valley of GaAs, *Phys. Rev. B* **93**, 161203 (2016).
- [45] H. Jani, L. Chen, and L. Duan, Pre-emission study of photoelectron dynamics in a GaAs/AlGaAs photocathode, *IEEE J. Quantum Electron.* **56**, 1 (2020).
- [46] L. Bányai, Q. Vu, B. Mieck, and H. Haug, Ultrafast Quantum Kinetics of Time-Dependent RPA-Screened Coulomb Scattering, *Phys. Rev. Lett.* **81**, 882 (1998).
- [47] K. El Sayed, S. Schuster, H. Haug, F. Herzel, and K. Henneberger, Subpicosecond plasmon response: Buildup of screening, *Phys. Rev. B* **49**, 7337 (1994).
- [48] R. Huber, F. Tauser, A. Brodschelm, M. Bichler, G. Abstreiter, and A. Leitenstorfer, How many-particle interactions develop after ultrafast excitation of an electron-hole plasma, *Nature* **414**, 286 (2001).